coatings

MDPI

Article

The Wavelet Transform for Feature Extraction and Surface Roughness Evaluation after Micromachining

Daniel Grochała *, Rafał Grzejda, Arkadiusz Parus and Stefan Berczyński

Faculty of Mechanical Engineering and Mechatronics, West Pomeranian University of Technology in Szczecin, 19 Piastow Ave., 70-310 Szczecin, Poland; rafal.grzejda@zut.edu.pl (R.G.); arkadiusz.parus@zut.edu.pl (A.P.); stefan.berczynski@zut.edu.pl (S.B.)

* Correspondence: daniel.grochala@zut.edu.pl

Abstract: Miniaturization is a dominant trend in machine building which requires the use of advanced techniques of manufacturing and control. Apart from dimensional and shape precision of miniaturized components, surface geometry, particularly roughness and so-called microroughness that results from the use of advanced treatment techniques, plays an important role in correct assembly, reliable operation and durability of the whole machine. The selection of filtration method in surface geometry of micro-objects can be a substantial problem. The authors of the paper propose to use wavelet filtration in digital processing of a point cloud to remove measurement noise and not to change the surface character of the measured object. Also, the authors propose, in this paper, some criteria for selecting the number of wavelet filtration levels based on minimalization of the RMS value. It is supposed to improve the efficiency of low-pass filtration of small areas of the surface, particularly compared to traditional λs Gaussian filtration.

Keywords: surface metrology; surface modeling; filtration; wavelet; micro-object coatings

Citation: Grochała, D.; Grzejda, R.; Parus, A.; Berczyński, S. The Wavelet Transform for Feature Extraction and Surface Roughness Evaluation after Micromachining. *Coatings* **2024**, *14*, 210. https://doi.org/10.3390/coatings14020210

Academic Editor: Sae Chae Jeoung

Received: 12 January 2024
Revised: 2 February 2024
Accepted: 4 February 2024
Published: 6 February 2024

1. Introduction

Micromechanical and microhydraulic solutions are frequently applied in modern machines used in medicine, aviation, and automotive industries. Micromechanical systems are responsible for the operation of optical and inductive sensors in measurement and research equipment. Devices that are assembled comprise components that work together, which have many functional surfaces, usually connected by multibolted connections [1–3]. Their surface geometry can limit or allow implementation of a number of specific tasks, including the ability to reflect or diffuse light and the ability to retain liquid, and it can also effect hydrophobic/hydrophilic properties of coatings [4,5]. The durability and reliability of micromachines and devices is also determined by their surface geometry. Apart from the well-known production techniques of microcomponents and devices, there are also several microtreatment technological processes [6–14].

The most frequent processes applied in industry and discussed in the literature are micromilling [6,7], microgrinding [10–12], micropolishing [13,14], different microlaser treatments [14,15], and so-called microhybrid treatment methods [16].

One of the most frequent problems is assessment of manufactured microsurfaces. The literature contains many approaches to the analysis of recorded surface geometry data. One typical approach is to determine surface geometry parameters for raw point data (without filtration) [17]. This approach requires the use of advanced measurement equipment, whose errors are negligibly small and do not generate distortion in the form of so-called measurement noise.

Another approach, which is the most frequent technique, is to use standard filtration methods that comply with the various parts of ISO 16610 [18–28], e.g., Gaussian filter [29–31]. In this approach, the conditions are set according to standards defined in the past which are still valid ISO 3274 [32].

The last approach used to process data recorded on surfaces is the so-called multiscale analysis. It relies on multiple-scale extraction of data with various filtration methods, depending on the operator's needs [33–36]. Multiscale analysis is difficult to conduct. It requires advanced knowledge of metrology and specialist software, and results can be difficult to interpret. Filtration procedures need a thorough description of all the stages of the process and their conditions.

There are some difficulties when measuring and investigating the properties of small surface areas (after micromachining of aluminum and steel). The use of standard filtration conditions (Table 1) is a certain way to ensure reproducibility and mutual ability to compare obtained results.

Table 1. Recommended conditions for measurement of surface profiles under ISO 3274 [32].

Filtration Recommendations for Profile Points			Recommendations Regarding Acquisition of Profile Points		
Expected Surface Roughness	Low-Pass Filter Measurement Noise	High-Pass Filter of Roughness			
Ra (µm)	λs (µm)	λc (µm)	*lt* [1] (mm)	*ln* [1] (mm)	*lr* [1] (mm)
>0.006 . . . 0.02	2.5	0.08	0.48	0.40	0.08
>0.02 . . . 0.1	2.5	0.25	1.5	1.25	0.25
>0.1 . . . 2	2.5	0.8	4.8	4.0	0.8
>2 . . . 10	8	2.5	15	12.5	2.5
>10 . . . 80	25	8.0	48	40	8.0

[1] Labels: *lt*—mapping section (including acceleration and deceleration of measurement sensor); *ln*—measurement section (multiple *n* of elementary section *lr*); *lr*—elementary section.

The above set of recommendations (Table 1) is sometimes the source of misunderstanding when 2D filtration conditions are translated into 3D surface filtration. This can be particularly the case when the size of the measured surface is significantly different from the length of the recommended profiles. Constraints can occur in filtering a surface of small size, where the length in different directions (X and Y axes) is smaller than 0.5 mm ($lt < 0.48$ mm). An additional constraint is the functional character of prepared waviness, from which only roughness should be extracted. This problem is illustrated in Figure 1 (from personal research), which shows a surface with the dimensions of X = 99 µm and Y = 99 µm, scanned (in plane XY) on a Mitutoyo quick-Vision HYPER WLI (Mitutoyo, Kanagawa, Japan). The measuring system (white light interferometric) is fixed-objective, with a range to 1.2 mm, magnification ×25, and numerical aperture of 0.5 with the resolution of 0.2 µm, and generated a dataset comprising 0.245 million points.

The surface of the specimen, shown in Figure 1a, was made by selective sintering of metallic powders (LPBF) from Inconel 718 alloy [37,38]. Machining was carried out on a custom SNTM-CM-ZUT-1 machine [39] using a JS512015F2C.0Z2-NXT (Seco Tools, Fagersta, Sweden) double-blade carbide cutter with a diameter of 1.5 mm and a helical line angle of the blade = 46°. The feed rate for micromilling was carried out according to the direction of the trajectory of laser sintering of the last layer. The cutting test was carried out at a speed of v_f = 24.0 m/min and a depth of cut of a_p = 100 µm. In Figure 1, the X direction is the feed direction, while the Y direction is the drilling direction. The presented surface contains heights that play the role of function as well as microroughness, whose value is difficult to determine (prefilter), according to the conditions (Table 1).

According to the procedure recommended by ISO 3274 [32], roughness should be determined with the low-pass filter λs = 2.5 µm, and the high-pass filter λc = 0.25 µm should be used to remove waviness errors (shape errors). There is some ambiguity to interpretation of results. A metrologist would think about roughness in terms of surface represented in a 2D image (filtered and rejected as noise). However, when we want to determine the functionality (i.e., height, shape, and volume) of manufactured waviness, we think about the surface—Figure 1a. The height of regular structures (Sp and Sv) in Figure 1a is about 2 µm. Between the presented extreme situations, it is permissible to use other

normalized filters with the length of λs and λc = 0.8 µm as well as λs and λc = 0.25 µm. In each case when a filter was used, surface geometry amplitude parameters were significantly different—see Table 2.

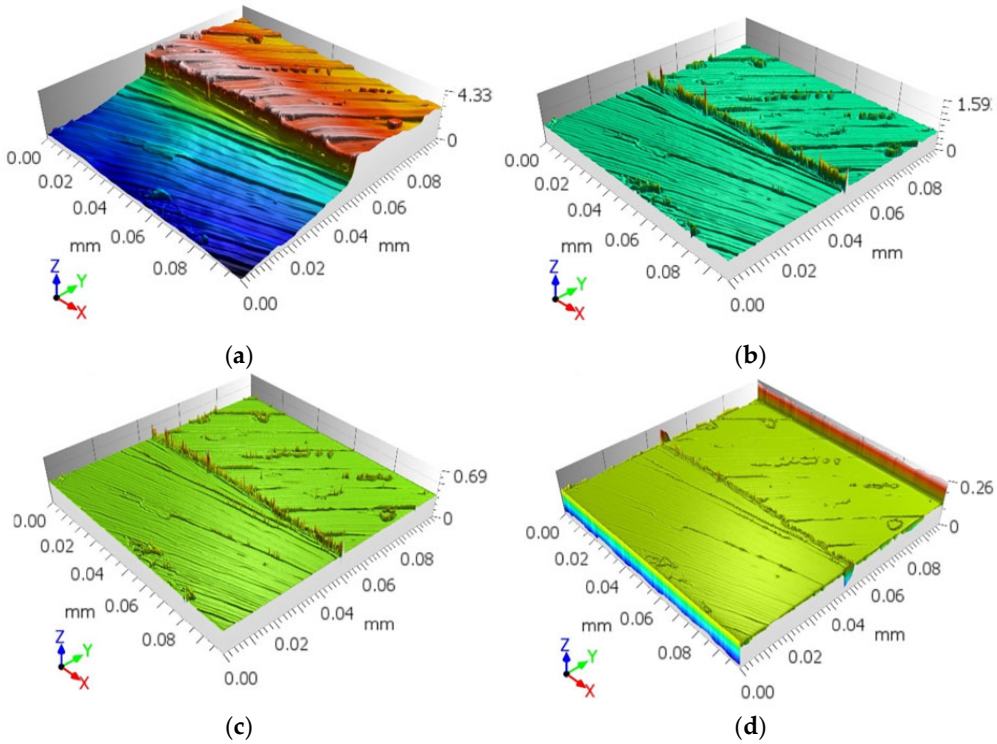

Figure 1. An example of functional surface after micromilling, from which roughness was extracted with high-pass Gaussian filter: (**a**) no filtering (raw surface); (**b**) for λc = 2.5 µm; (**c**) for λc = 0.8 µm; (**d**) for λc = 0.25 µm.

Table 2. Surface roughness after micromachining determined with high-pass Gaussian filter.

Parameter	Roughness Values after Using High-Pass Gaussian Filter			
	Raw Surface	λc = 2.5 µm	λc = 0.8 µm	λc = 0.25 µm
Sq (µm)	1.262	0.034	0.011	0.007
Sa (µm)	1.183	0.015	0.003	0.001
Sp (µm)	2.115	1.015	0.365	0.133
Sv (µm)	2.223	0.577	0.325	0.135
Sz (µm)	4.338	1.593	0.691	0.268

It is becoming difficult to select commonly available standard lengths of λ filter that would allow the separation of measurement noise or the extraction of microroughness without changing the character of the functional surface core.

The problem of proper selection of filter length and, therefore, the problem of filter affecting the points of surface core occurs regardless of filtration type (Gaussian, spline, and coarse Gaussian) [30,33–36,40–42]. The scale of that phenomenon decreases as the height of surface geometry and the area of measured surface increase.

The literature also describes a method called wavelet transform. The advantage of the method is that it can separate roughness (measurement noise and/or microroughness) of functional surfaces with a regular shape [40,41,43,44]. This property is particularly important in surface metrology, in the assessment of milling stability [45–47], and in other areas of technology regarding machine components [48,49]. Wavelet analysis is often used in processing surface signals obtained in typical auxiliary technological operations, such as the assessment of washing efficiency and dirt removal [50], and the assessment of quality

of paint coatings and their reflectivity. For filtration of small surfaces, authors apply not only wavelet transform [51] but also combined methods of multiscale filtration [52].

2. Detection of Measurement Noise

Two filters are commonly used to process 3D signal from surface geometry measurement: Gaussian filters [25] and Gaussian regression filters [27]. They have both evolved from filtration of 2D signal collected from surface profiles, i.e., from Gaussian filter according to ISO 16610-21 [18]. Apart from Gaussian filtration, other methods are used [53–56] to detect and remove high-frequency components of so-called noise. Surface [54] and adaptive filtering [53] has become particularly popular. The use of any filtration method, including wavelet filtration [43–50], poses a challenge for every metrologist. He/she must select a way in which the filter will operate (filter value/length) and stop [57].

Noise Extraction Method Based on Subtraction of Random Variables

The aim is to separate noise while at the same time not change the character of surface of the measured object. Statistical analysis of the recorded measurement data bank can be useful in determination of filtration stoppage:

$$Zm_1 = Surf + Snoise_1 \text{ and } Zm_2 = Surf + Snoise_2 \quad (1)$$

where $Surf$—constant value related to measured coordinates $\left(Surf_{(X;Y;Z)}\right)$; Zm_1; Zm_2—random variables of the coordinates of surface Z height; $Snoise_1$; $Snoise_2$—random variables of measurement noise (that accompany the measurement of Zm surface coordinates).

The difference of the random variables of the coordinates of the height of the Z surface is equal to

$$Zm_1 - Zm_2 = Snoise_1 - Snoise_2 \quad (2)$$

Assuming a certain natural changeability of the analyzed property of surface $Surf$, it can be expressed with natural variance of variables:

$$Var(Zm_1 - Zm_2) = Var(Snoise_1) + Var(Snoise_2) \quad (3)$$

Under the assumption that the unchanging conditions of measurement are

$$Var(Snoise_1) = Var(Snoise_2) = \sigma^2_{noise} \quad (4)$$

after substituting Equation (4) into Equation (3), we obtain

$$Var(Zm_1 - Zm_2) = 2\sigma^2_{noise} \quad (5)$$

Hence, the value of measurement noise in many measurements of the same surface fragment can be determined in the following form:

$$\sigma_{noise} = \frac{1}{\sqrt{2}} \cdot \sqrt{Var(Zm_1 - Zm_2)} \quad (6)$$

ISO 25178-2 [58] defines many surface topography parameters, including Sq, i.e., the value of root-mean-square deviation of surface Zm points from the mean height. Because of its analogy to RMS (root-mean-square) in signal analysis, the Sq parameter is often used in the analysis of surface topography. Taking Sq^2 as a random variable, we can write

$$Sq^2 = \frac{1}{N}\sum_{i=1}^{n}(z_i + \xi_i)^2 \quad (7)$$

Given the constant positioning of coordinates x_i and y_i (the same fragment of measured surface), measurement noise is generated only through the changes of coordinates z_i. The

value of Sq^2 (i.e., variance of coordinates z_i), using the formula for the square of the sum, can be calculated as

$$Sq^2 = \frac{1}{N}\sum_{i=1}^{n}\left(z_i^2 + 2z_i\xi_i + \xi_i^2\right) \tag{8}$$

If noise ξ_i, for the values of coordinates z_i, has distribution $\mu(\xi) = 0$ and variance $var(\xi) = \sigma^2(\xi)$, then

$$E(Sq^2) = E\left(\frac{1}{N}\sum_{i=1}^{N} z_i^2 + \frac{2}{N}\sum_{i=1}^{N} z_i\xi_i + \frac{1}{N}\sum_{i=1}^{N} \xi_i^2\right) \tag{9}$$

After transformations, we can write that the mean value of Sq of the analyzed surface property together with measurement noise is

$$E\left(Sq^2\right) = Sq_{surf}^2 + \sigma^2(\xi) \tag{10}$$

To check whether the concept of rejecting measurement noise is correct, a series of experiments was conducted in which the same fragment of surface was measured many times. An AltiSurf A520 multisensor (Altimet, Thonon-les-Bains, France), fitted with achromatic confocal CL1 sensor, with a measuring range of 130 µm and optical resolution of 8 nm [59], was used in the experiments. Measurements were made on roughness standard with nominal values of Ra = 3.2 µm and Rz = 10 µm (see [60] for comparison). The standard did not contain any specification of stereometric parameters Sa or Sq. A measurement area with the size of 1.0 × 1.0 mm was determined for the standard. The scanning resolution was determined experimentally to be 0.47 µm in the X axis and 0.47 µm in the Y axis, which yielded over 4.4 million mapping points for each of five surfaces—see Figure 2.

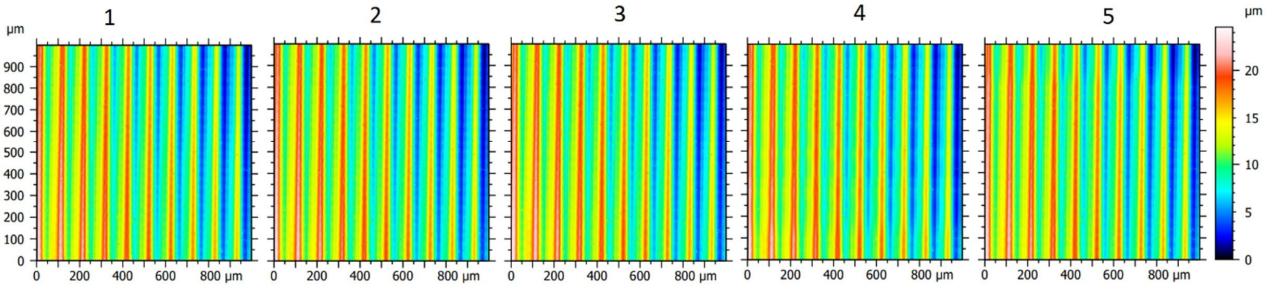

Figure 2. Surface of roughness standard measured five times in the same place.

At the next step, measured areas were subtracted from each other using AltiMap PREMIUM 6.2 (Altimet, Thonon-les-Bains, France). The image obtained after subtracting the difference (in the form of measurement noise) is presented in Figure 3.

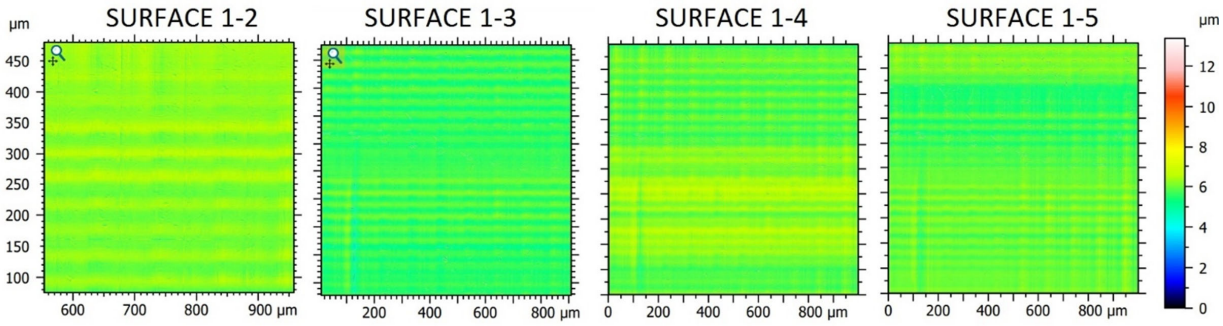

Figure 3. Surfaces that show measurement noise resulting from subtracting successive surfaces from surface No. 1.

Measurement noise was determined in the same way in all systems. Reference surface was successively changed when the values of coordinates z_i were subtracted from the successive surface [57]. The root-mean-square (RMS) powers of measurement noise determined by subtracting surface are presented in Table 3.

Table 3. The root-mean-square power of measurement noise determined by subtracting surface.

RS No.	*Sq* (µm)	$\overline{\sigma}_{noise}$ (µm)	Noise (RS-MS) [1] (µm)				
			MS No. 1	MS No. 2	MS No. 3	MS No. 4	MS No. 5
1	3.64	0.231	–	0.260	0.237	0.207	0.221
2	3.74	0.196	0.260	–	0.163	0.229	0.237
3	3.73	0.199	0.237	0.163	–	0.224	0.207
4	3.74	0.239	0.207	0.229	0.224	–	0.221
5	3.76	0.231	0.221	0.237	0.207	0.221	–

[1] Labels: RS—reference surface; MS—measured surface.

During the numerical experiment, the mean value of measurement $\overline{\sigma}_{noise}$ was determined to be 8.2% of *Sq* of the measured surface. Noise filtration conducted in this way is time-consuming. The surface needs to be measured in the same way at least twice (the same coordinates X and Y of the measured surface). It is very difficult to keep constant conditions of measurement in the industrial context. Furthermore, during multiple measurements, a random factor can occur which would affect the measured object by changing its surface. In the experiment, the scan of one measurement area took approximately 4 h. The value of measurement noise determined in this way will always be significantly overestimated [57,61]. Apart from changeability that is caused only by the measurement system, there are other sources of change linked to the environment and the measured object. The solution to the problem of noise determination in single surface measurement can be the use of adaptive filtration methods. Kingsbury's dual-tree complex wavelet transform can be one of these methods.

3. Examination of Adaptive Wavelet Filtering

The very important part of the surface roughness measurement is a proper determination of filtration parameters. This stage is fully dependent on the operator's experience and qualifications and may result in obtaining different results for the same surface when analyzed by different operators. The situation becomes more complicated when we consider measurement noise, usually high frequency in optical measurements. The noise should be filtered out. The filtration process must not disturb the result of the parameters of the measured surface. There are many suggestions for signal processing in the literature [62]. The use of wavelet transform is one of the most effective methods that has been intensively explored in recent years [46,63–65]. Authors examine many types of wavelets, and complex Kingsbury's type was chosen, because of its good ability to reject the various noise from data point clouds. Kingsbury's wavelet is a complex one and, thus, is insensitive to the shift signal in measured data. Many other researchers have used this type of wavelet in noise-filtering problems [46,62–68]. In wavelet transform, the signal is decomposed into low-frequency approximation and a set of higher-frequency details corresponding to each level. In [46], the authors compared the multiscale wavelet transforms to other noise-filtering methods, such as principal component analysis (PCA), discrete cosine transform (DCT), and Fourier transform (FT). The filtration process could be performed by removing data from each selected level by soft or hard thresholding. In [67], the "universal threshold" was proposed $\sqrt{2\log(n)}\sigma/\sqrt{n}$ for Gaussian noise with standard deviation σ and signal size n. However, this method could cause errors at the synthesis stage for dual-tree wavelet (DTW) transform. Discrete wavelet transform (DWT) with dyadic scale is often used in

surface analysis [66], in which the signal $z(x)$ could be decomposed in terms of wavelet ψ and scaling function ϕ according to

$$z(x) = \sum_{n=-\infty}^{\infty} c(n)\phi(x-n) + \sum_{j=0}^{\infty}\sum_{n=-\infty}^{\infty} d(j,n)2^{\frac{j}{2}}\psi\left(2^j x - n\right) \tag{11}$$

$$\mathrm{c}(n) = \int_{-\infty}^{\infty} z(x)\phi(x-n)\mathrm{d}t \tag{12}$$

$$d(j,n) = 2^{\frac{j}{2}}\int_{-\infty}^{\infty} z(x)\psi\left(2^j x - n\right)t \tag{13}$$

where $c(n)$—scaling coefficients; $d(j,n)$—wavelet coefficients; j—scale factor (decomposition level); n—shift.

Due to the simplicity of applying the DWT algorithm, it is often implemented (Figure 4) with a set of low-pass (LP) and high-pass (HP) filter banks [66] with downsampling/upsampling of the signal by a factor of 2. This structure is called dual-tree wavelet transform (DTWT), and with appropriately chosen filters, it is very close to an analytic solution, even for relatively short filters [66]. The main drawback is 2× redundancy.

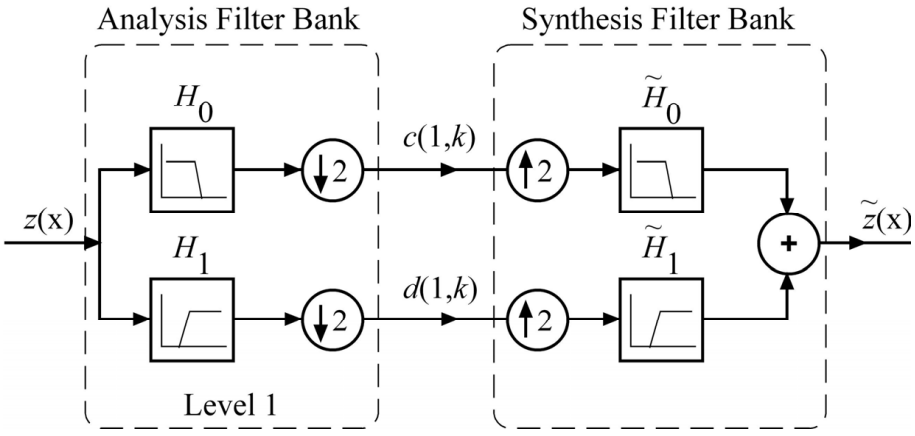

Figure 4. Wavelet transform of signal $z(x)$ using LP/HP filter banks (H_0, H_1—low/high-pass analysis filter, $\widetilde{H}_0$, $\widetilde{H}_1$—low/high-pass synthesis filter, $\widetilde{z}(x)$—reconstructed signal, $d(1,k)$, $c(1,k)$—wavelet and scaling coefficients for level 1).

The use of wavelet transformation involves an important issue that may lead to disadvantages, and which, therefore, should be considered [68]. As wavelet coefficients tend to oscillate around zero, there is a problem with comparing results and classifying signal parameters based on wavelet coefficients. The next problem is wavelet coefficient sensitivity to signal shift. In [68], it was shown that wavelet transform results were significantly different for signal $z(x)$ and the same signal shifted by $\Delta x : z(x + \Delta x)$. This property also makes it difficult to compare the results of wavelet transform of two signals. It is not known what causes the differences: amplitude properties of the signal or signal shift. One way to deal with these problems is to use complex wavelet transform (CWT), as in [68]. For a discrete signal as surface measurement, the most convenient way is to use dual-tree complex wavelet transform (DTCWT) [13]. This idea could be implemented by using two sets of real LP/HP filter banks. The first set of filter banks is used for calculating the real part, and the second one is used for the imaginary part of wavelet coefficients, as in Figure 5.

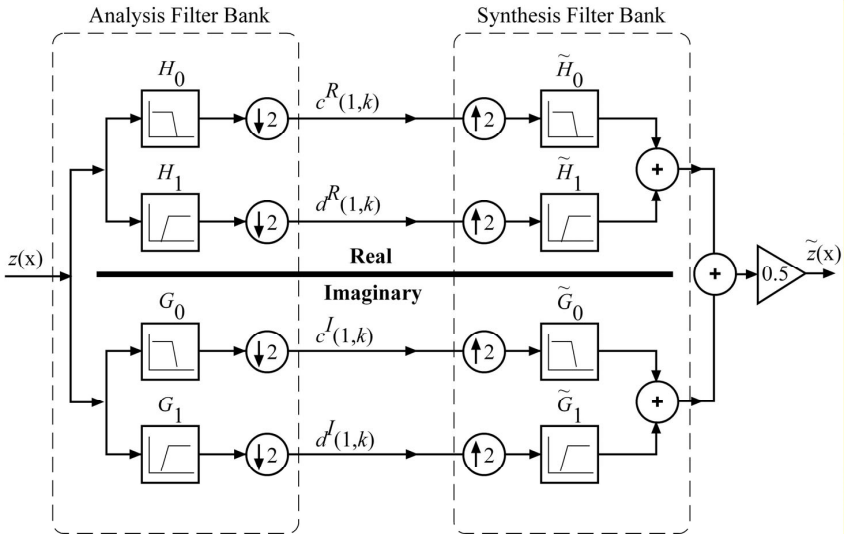

Figure 5. Wavelet transform of signal $z(x)$ using two sets of real LP/HP filter banks (H_0, H_1—low/high-pass analysis filter (real part), $\widetilde{H}_0$, $\widetilde{H}_1$—low/high-pass synthesis filter (real part), G_0, G_1—low/high-pass analysis filter (imaginary part), $\widetilde{G}_0$, $\widetilde{G}_1$—low/high-pass synthesis filter (imaginary part), $\widetilde{z}(x)$—reconstructed signal, $d^R(1,k)$, $c^R(1,k)$—wavelet and scaling coefficients for level 1 (real part), $d^I(1,k)$, $c^I(1,k)$—wavelet and scaling coefficients for level 1 (imaginary part)).

The filters in real trees and imaginary trees are designed to satisfy the perfect reconstruction condition and form the Hilbert transform. Since all filters are real numbers, the Hilbert transform could be applied with a half-sample shift between input signals for both trees. Finally, even samples of input signal go to one tree and odd ones to the second one. More details about the filter design method and its properties can be found in [68].

3.1. Examination of Adaptive Filtration Method Using Mathematical Formulae

In this section, the surface geometry parameters (SGPs) determined for a numerically generated roughness profile are presented and compared to the analytical solution. The proposed wavelet-based SGP calculation method is compared to the standard Gauss filtering process. The main advantages of the proposed method are summarized.

3.1.1. SGPs of the Analytically Generated Roughness Profile of the Ideal Surface

Analytical roughness of the ideal flat surface is described by

$$z_a(x,y)\begin{cases} x = [7\sin(2\ \pi\ 100\ x)], & x \in \langle 0:1000,\ 0.0005\rangle(\mu\text{m}) \\ y & y \in \langle 0:1000,\ 0.0005\rangle(\mu\text{m}) \end{cases} \quad (14)$$

For simplification, the case with roughness profile only in the x direction is analyzed. The geometrical parameters are obvious and therefore are omitted. The root-mean-square value is calculated using

$$Sq = \frac{7}{\sqrt{2}} = 4.9497 \quad (15)$$

where Sq is calculated and valid for the full wavelength signal.

3.1.2. SGPs of the Discretized Roughness Profile of the Ideal Surface

Parameters of the analytical signal are similar to the real master, which will be analyzed in Section 2 (Table 3). Results obtained from a confocal microscope via the built-in acquisition system are always discretized. The discretization step size is dependent on the type of measurement machine and varies from 0.02 to 0.5 µm. For easy comparison with real measurement, the analytic signal is discretized with a step of 0.4760 µm. The signal

and calculated SGPs are presented in Figure 6 and Table 4. Those values will be used as reference parameters in further analysis.

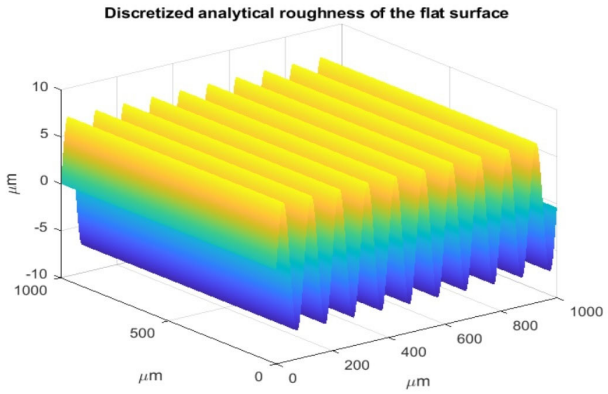

Figure 6. Discretized analytical roughness of the flat surface (wavelength 100 μm, amplitude 7 μm, discretization step size of 0.4760 μm).

Table 4. Calculated surface parameters of the numerical master and master surfaces with brown noise.

Parameter	Description	Master Value	Master Value with White Noise	Master Value with Brown Noise
Sq (μm)	RMS deviation of the surface	4.9507	4.9763	4.9967
Sp (μm)	Maximum surface peek height	7.0000	9.3947	8.7055
Sv (μm)	Lowest valley of the surface	7.0000	9.3712	8.6092
Sz (μm)	Maximum height of topographic surface	14.0000	18.7658	17.3147
Sa (μm)	Arithmetic mean deviation	4.4581	4.4695	4.4845
St (μm)	Total height of surface	14.000	18.7658	17.3147

3.1.3. SGPs of the Discretized Roughness Profile with Simulated Measurement Noise

To move analysis toward the real results, the analytic signal will be affected by various types of noise. Figure 7 present a discretized signal with white and brown noise $z_n(x,y)$. The calculated SGPs for each signal are presented in Table 4.

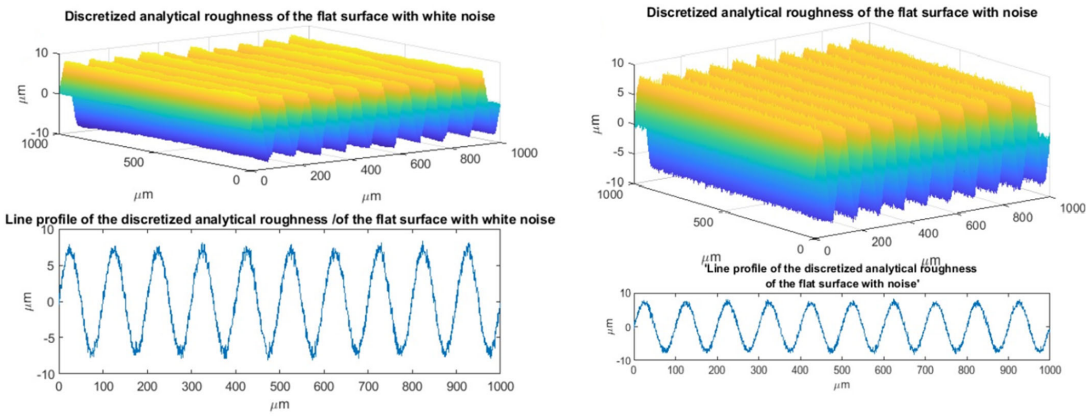

Figure 7. Discretized analytical roughness of the flat surface with standard deviation noise, and zero mean value, Gaussian distribution for (**a**) 0.5 μm white noise and (**b**) 0.5 μm brown noise.

It is easy to compare results from Table 4. One can see that the SGPs are significantly affected by the measurement noise. In the further sections of this paper, the effective

method to determine correct values of SGPs from noised signal, according to Equation (10), will be presented. The method is based on the wavelet analysis, whose parameters depend on the root-mean-square value of the analyzed signal at each level of wavelet transform.

3.1.4. Proposed Method of SGP Calculation Based on Wavelet Analysis

The wavelet analysis is a multilevel transformation process. The number of levels depends on the type of signal (low or high frequency) and there are no obvious rules to determine how many levels are necessary to reject the disturbance noise from the measured roughness profile to calculate the correct values of surface parameters. This is a typical problem of wavelet analysis in the measurement process. Results obtained by researchers are dependent on the wavelet type and number of analyzed levels. In this paper, the authors propose to make the number of levels dependent on the RMS value (Figure 8).

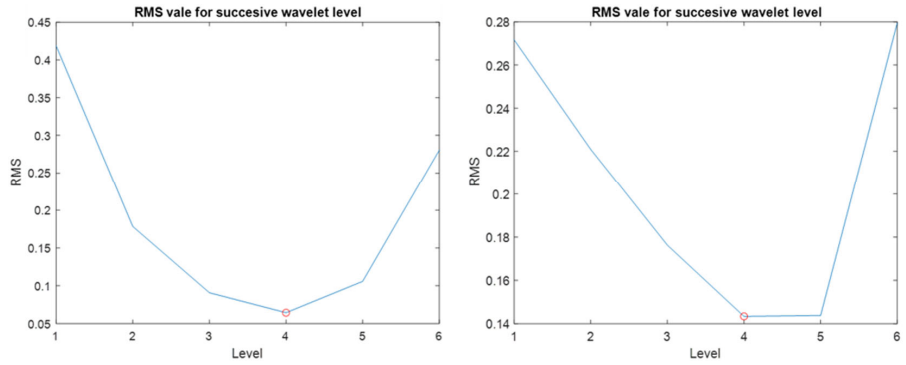

(**a**) (**b**)

Figure 8. RMS value determined independently for 6 levels of wavelet transform for signal with: (**a**) white noise—red point indicates the suggested number of levels = 4; (**b**) brown noise—red point indicates the suggested number of levels = 4.

RMS is calculated independently for each level of transformation. Wavelet analysis, as a low-pass filtering process, rejects high-frequency measurement noise from the signal on successive levels. This process could be clearly observed in declining RMS value.

The red point at which an RMS increase could be observed is caused by partial leakage signal from the roughness band to the noise band. This means that the correct number of wavelet levels is 4. A deeper-level analysis will lead to incorrect results. The results of filtering roughness profile with 4 levels of wavelet transform ($z_w(x,y)$) are presented in Figure 9. The calculated SGPs are presented in Table 5.

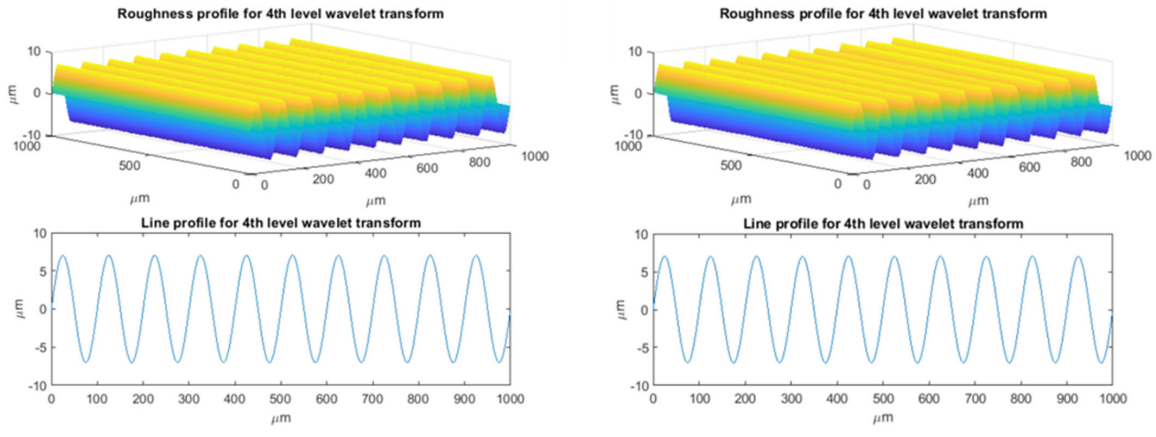

(**a**) (**b**)

Figure 9. Results for 4th-level wavelet analysis for signal with (**a**) white noise; (**b**) brown noise.

Table 5. Roughness parameters and parameters calculated for 4th-level wavelet analysis for signal with white and brown noise.

Parameter	Description	Master Value	Master Value with White Noise	Master Value with Brown Noise
Sq (µm)	RMS deviation of the surface	4.9507	4.9503	4.9730
Sp (µm)	Maximum surface peek height	7.0000	7.2153	7.4219
Sv (µm)	Lowest valley of the surface	7.0000	7.2185	7.4115
Sz (µm)	Maximum height of topographic surface	14.0000	14.4338	14.8334
Sa (µm)	Arithmetic mean deviation	4.4581	4.4575	4.4475
St (µm)	Total height of surface	14.000	14.4338	14.8334

If the signal $z_w(x,y)$ presented in Figure 9 is subtracted from the original $z_n(x,y)$ noised signal (Figure 8), the measurement noise $n(x,y)$ can be determined. The standard deviation of determined noise (acc. Equation (10)) signal is equal to 0.5012 µm and 0.4740 µm for white and brown noise, respectively. In Figure 10, the normal probability plot and noise distribution plot are presented.

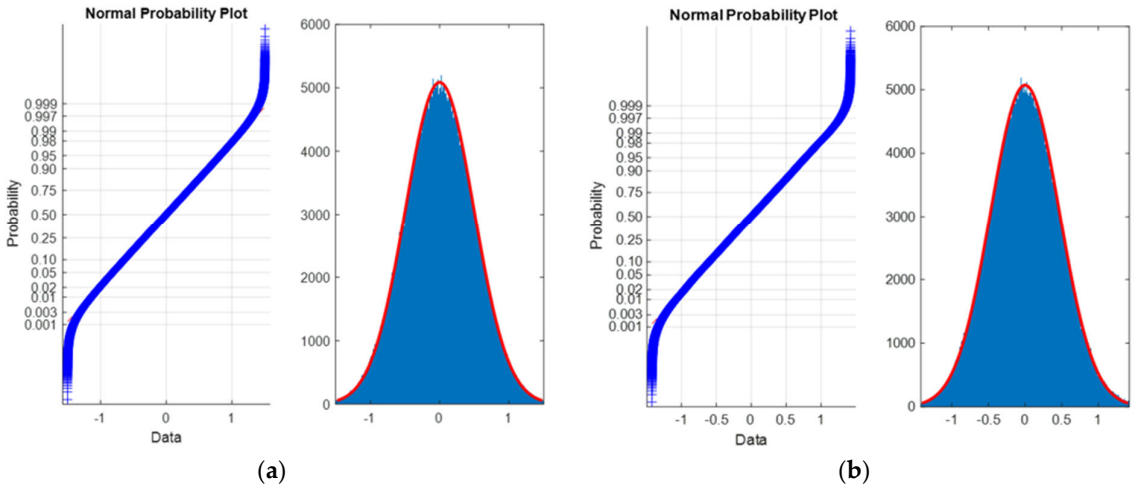

(**a**) (**b**)

Figure 10. Normal probability plot and distribution of determined noise signal after 4th-level wavelet transform for signal with (**a**) white noise; (**b**) brown noise.

Using the wavelet transform to subtraction noise, a result of the nominal values of the pattern SGPs were not obtained exactly. The differences not exceeding 3% of the amplitude values of the parameters (such as *Sp*, *Sz*, *Sv*, *St*) were within the nominal value of the parameter with $\pm 2 \cdot Snoise$ (95% confidence interval for a single observation).

The obtained results were very close to the original noise parameters: 0.5 µm standard deviation and normal distribution. On this basis, it was proved that the assumed number of wavelet levels was correct, and the measurement noise was successfully rejected from the measurement signal without significantly affecting the SGPs. The proposed method effectively reduced the influence of noise in the measurement signal for both cases. Brown noise is a lower-frequency energy signal in comparison with white noise. Wavelet transform could be treated as a low-frequency filtering process. A part of low-frequency noise can pass the filtering process; therefore, the standard deviation of the determined noise is lower than 0.5 µm, especially for a brown noise signal.

3.2. Examination of Adaptive Filtration Method Using a Material Standard of Roughness

In this paper, the authors propose a method to define the number of wavelet levels used in noise filtering of measured data. This is a crucial point in wavelet filtering

application—using a high number of levels leads to corruption of the results and "destroys" the original shape of the surface. Therefore, the minimum RMS criterion, calculated for data at each level of wavelet transformation, was chosen as a correct number of levels. In the results, the noise is rejected at a high ratio without distortion of the original surface. Moreover, this method allows assessment of the uncertainty of the determined profile parameters (roughness, etc.). The effectiveness of the proposed method was proved by comparison with results published online by National Institute of Standards and Technology (NIST).

The idea of adaptive wavelet filtering with RMS minimization (for *Sa* parameter of the filtered rest) was used to process a point cloud recorded in the measurement of real standard of roughness (see the red circle in Figure 11). The method was compared to the standard methodology used for processing small surfaces, in line with ISO 3274 [32]. The length of elementary section was *le* = 200 µm and *n* = 6 (Figure 11).

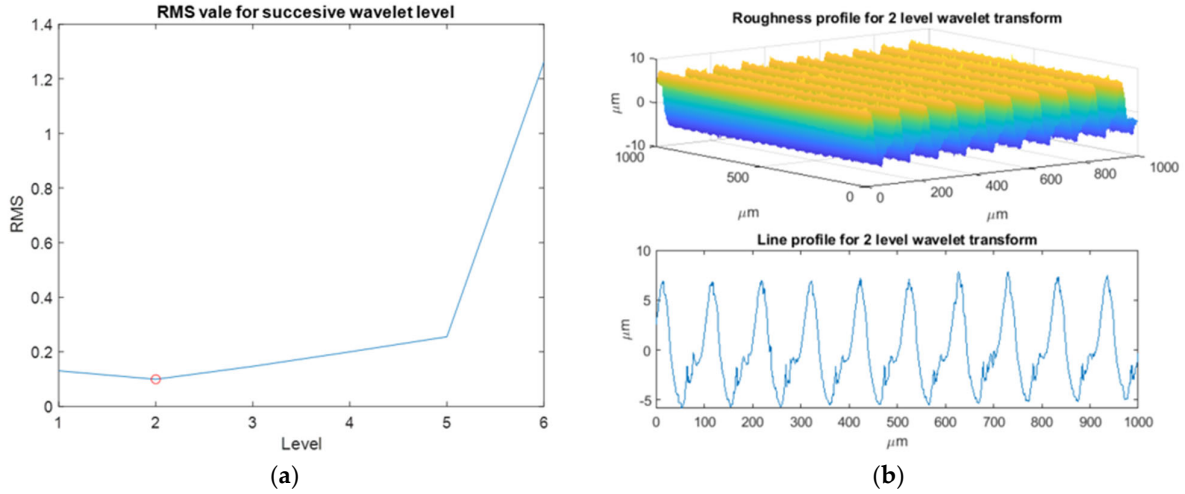

Figure 11. Subtraction of measurement noise from the surface of material roughness standard: (**a**) RMS values after wavelet transform; (**b**) view of filtered surface.

The obtained results are presented in Table 6.

Table 6. Roughness parameters calculated for wavelet transform and Gaussian filtering on roughness standard.

Parameter	Description	Raw Master Value	After Wavelet Filtering	After Gaussian Filtering (250 µm)
Sq (µm)	RMS deviation of the surface	3.7874	3.7826	2.5796
Sp (µm)	Maximum surface peek height	9.4247	9.1543	7.3722
Sv (µm)	Lowest valley of the surface	7.2324	6.7996	5.8757
Sz (µm)	Maximum height of topographic surface	16.6571	15.9539	13.2479
Sa (µm)	Arithmetic mean deviation	3.1822	3.1804	2.1088
St (µm)	Total height of surface	16.6571	15.9539	13.2479

4. Discussion on SGP Calculation Method Based on Wavelet Analysis and Subtraction of Random Variables

The application of the developed wavelet filtration methods to the surface after micromilling (Figure 1a) allows the identification and removal of measurement noise already from a single measurement—see Figure 12a. This is a very favorable situation in which there are no additional sources affecting the variability of the measured object, and the measurement uncertainty (U_{Kin}) is within the Sq_{noise} (RMS) value. On the other hand,

parameter values measured on small areas of the surface are not distorted by "too strong" Gaussian filtering (established based on guidelines in ISO 3274 [32]).

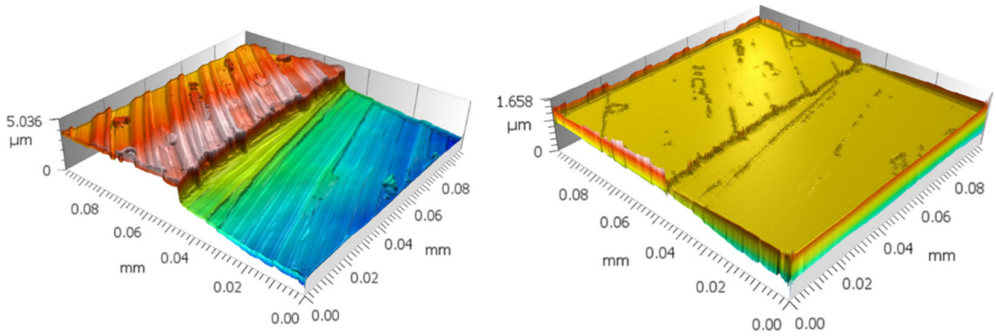

(**a**) (**b**)

Figure 12. Example of functional surface after micromilling which roughness was extracted with wavelet transform (1 level): (**a**) surface after denoising; (**b**) noise.

The noise minimum, which includes the measurement uncertainty for the analyzed case of the functional surface, already occurred after applying the first Kinsburry filtering level. The values of the roughness parameters obtained during the verification tests, as well as the uncertainty of the *Sq* parameter, are provided in Table 7.

Table 7. Surface roughness after micromachining determined with high-pass Gaussian filter and wavelet transform.

Parameter	Values after Using High-Pass Gaussian Filter and Wavelet Transform			
	Raw Surface	Gaussian λc = 2.5	Kinsburry 1-Level	U_{Kin} (µm)
Sq (µm)	1.262	0.034	1.261	±0.030
Sa (µm)	1.183	0.015	1.182	±0.006

Filtration of point clouds is crucial to improve the image of a measured object. However, "defiltering" should not change the object's character and change its surface geometry parameters that define its function.

Although filtering that uses Gaussian methods is very common, it can introduce some ambiguity, particularly when using normalized values on the surface, where frequency and waviness amplitude change in a random way. Gaussian filters with normalized values do not "catch up" on small surface shapes which change dynamically.

The best effects to remove measurement noise are provided by methods of multiple measurement and subtraction of coordinates *Z*. However, they require a careful metrologist and stable measurement apparatus. It is difficult to maintain precision in multiple measurements of the same surface fragment. It is especially challenging in scanning measurements based on interference of white light phase shift or on confocal methods. This filtering method gave the expected good results. It seems that for objects produced by other chip or laser machining techniques, this method of removing errors will work well. It is possible to test and remove errors from the measurements of objects of organic origin as well as those manufactured from plastics and composite materials.

Measurement of surface topography (large areas) conducted with high horizontal resolution (*XY*) can last over 10 h. Therefore, the stability of environment in a lab is very difficult to maintain, and in industrial context, it is impossible.

The wavelet transform allows us to achieve a very high level of agreement of the values of the measured parameters of the surface, as shown by tests on analytical standards. It should be assumed for measurements of real surfaces at single measurements to achieve

comparable accuracies, i.e., errors of the estimated parameters in relation to the "real" greater than ±3%.

5. Conclusions

To summarize the paper, the following conclusions can be made:

1. The best method to remove measurement noise from small areas is to use wavelet filtering based on minimization of RMS of the signal (the values of *Sq* of the filtered rest). This filtration method allows the separation of noise in individual measurements (where values are the same). Additionally, it was proven with analytical methods, which were confirmed in practice, that the wavelet filtering method that uses so-called Kinsburry dual-tree complex wavelet transform can very well remove noise from small surface areas (without deforming the surface, as is the case in Gaussian filtering).
2. It can be assumed that technological surfaces of random (isotropic/anisotropic) morphology of any size *XY* and any resolution can be filtered with wavelet transform based on RMS signal minimization. However, during experiments it is important. The above observations require further experimental research. It remains to be checked whether the application of wavelet filtering can result in "defiltering" of unique surface features (such as tribological, hydrophobic, or hydrophilic properties).
3. Wavelet filtering can reduce the spread of surface geometry parameters. It is crucial when deciding which would enable unequivocal assessment of an object (especially when the value of the parameter under investigation is on the borderline: good/not good). In this way, the likelihood of escalating problems in the industry can be reduced.
4. Of the many methods for removing noise (errors of the measuring apparatus), the Kinsburry wavelet works best, and this is true regardless of the surface area and resolution adopted when scanning the surface. Once this phenomenon was explained, it was possible to use the developed filtering method and wavelet filter optimization in surface micromachining research. The results may be useful in other areas of technology and life sciences.

Author Contributions: Conceptualization, D.G.; methodology, D.G.; software, D.G. and A.P.; validation, D.G., A.P. and R.G.; formal analysis, D.G.; investigation, D.G. and A.P.; resources, D.G.; data curation, D.G.; writing—original draft preparation, D.G.; writing—review and editing, A.P., R.G. and S.B.; visualization, D.G.; supervision, S.B.; project administration, R.G.; funding acquisition, R.G. All authors have read and agreed to the published version of the manuscript.

Funding: This research received no external funding.

Institutional Review Board Statement: Not applicable.

Informed Consent Statement: Not applicable.

Data Availability Statement: The data presented in this study are available on request from the corresponding author.

Acknowledgments: Research was carried out on research apparatus purchased as part of the project No. RPZP.01.03.00 32-0004/18. Project co-financed by the European Union from the European Regional Development Fund under the Regional Operational Program of the West Pomeranian Voivodeship 2014-2020. Project co-financed by the Ministry of Education and Science.

Conflicts of Interest: The authors declare no conflicts of interest.

References

1. Grzejda, R. Modelling Nonlinear Multi-Bolted Connections: A Case of Operational Condition. In Proceedings of the 15th International Scientific Conference 'Engineering for Rural Development 2016', Jelgava, Latvia, 25–27 May 2016; pp. 336–341.
2. Grzejda, R. New method of modelling nonlinear multi-bolted systems. In *Advances in Mechanics: Theoretical, Computational and Interdisciplinary Issues*, 1st ed.; Kleiber, M., Burczyński, T., Wilde, K., Gorski, J., Winkelmann, K., Smakosz, Ł., Eds.; CRC Press: Leiden, The Netherlands, 2016; pp. 213–216.

3. Palenica, P.; Powałka, B.; Grzejda, R. Assessment of modal parameters of a building structure model. *Springer Proc. Math. Stat.* **2016**, *181*, 319–325.
4. Ba, Z.; Wang, Y.; Sun, T.; Jia, Y.; Zhang, L.; Dong, Q. Preparation and properties of hydrophobic micro-arc oxidation/layered double hydroxide composite coating on magnesium alloy. *Surf. Coat. Technol.* **2023**, *475*, 130113. [CrossRef]
5. Kumar, S.S.A.; Ma, I.A.W.; Ramesh, K.; Ramesh, S. The synergistic effects of graphene on the physical, hydrophobic, surface, and thermal properties of acrylic-epoxy-polydimethylsiloxane composite coatings. *Int. J. Adhes. Adhes.* **2024**, *128*, 103546. [CrossRef]
6. Brinksmeier, E.; Preuss, W. Micro-machining. *Philos. Trans. R. Soc. A Math. Phys. Eng. Sci.* **2012**, *370*, 3973–3992. [CrossRef] [PubMed]
7. Chen, T.-H.; Fardel, R.; Arnold, C.B. Ultrafast z-scanning for high-efficiency laser micro-machining. *Light Sci. Appl.* **2018**, *7*, 17181. [CrossRef] [PubMed]
8. Wan, M.; Wen, D.-Y.; Ma, Y.-C.; Zhang, W.-H. On material separation and cutting force prediction in micro milling through involving the effect of dead metal zone. *Int. J. Mach. Tools Manuf.* **2019**, *146*, 103452. [CrossRef]
9. Aslantas, K.; Danish, M.; Hasçelik, A.; Mia, M.; Gupta, M.; Ginta, T.; Ijaz, H. Investigations on surface roughness and tool wear characteristics in micro-turning of Ti-6Al-4V alloy. *Materials* **2020**, *13*, 2998. [CrossRef] [PubMed]
10. Aurich, J.C.; Engmann, J.; Schueler, G.M.; Haberland, R. Micro grinding tool for manufacture of complex structures in brittle materials. *CIRP Ann.* **2009**, *58*, 311–314. [CrossRef]
11. Kumar, S.P.L. Measurement and uncertainty analysis of surface roughness and material removal rate in micro turning operation and process parameters optimization. *Measurement* **2019**, *140*, 538–547. [CrossRef]
12. Setti, D.; Arrabiyeh, P.A.; Kirsch, B.; Heintz, M.; Aurich, J.C. Analytical and experimental investigations on the mechanisms of surface generation in micro grinding. *Int. J. Mach. Tools Manuf.* **2020**, *149*, 103489. [CrossRef]
13. Lee, P.-H.; Nam, J.S.; Li, C.; Lee, S.W. An experimental study on micro-grinding process with nanofluid minimum quantity lubrication (MQL). *Int. J. Precis. Eng. Manuf.* **2012**, *13*, 331–338. [CrossRef]
14. Guo, J.; Suzuki, H.; Higuchi, T. Development of micro polishing system using a magnetostrictive vibrating polisher. *Precis. Eng.* **2013**, *37*, 81–87. [CrossRef]
15. Nüsser, C.; Wehrmann, I.; Willenborg, E. Influence of intensity distribution and pulse duration on laser micro polishing. *Phys. Procedia* **2011**, *12*, 462–471. [CrossRef]
16. Chavoshi, S.Z.; Luo, X. Hybrid micro-machining processes: A review. *Precis. Eng.* **2015**, *41*, 1–23. [CrossRef]
17. Flucke, C.; Gläbe, R.; Brinksmeier, E. Diamond Micro Chiseling: Cutting of Prismatic Micro Optic Arrays. In Proceedings of the 7th International Conference—European Society for Precision Engineering and Nanotechnology, Bremen, Germany, 20–24 May 2007.
18. *PN-EN ISO 16610-21*; Geometrical Product Specifications (GPS), Filtration, Part 21: Linear Profile Filters: Gaussian Filters. Polish Committee for Standardization: Warsaw, Poland, 2013.
19. *PN-EN ISO 16610-22*; Geometrical Product Specifications (GPS), Filtration, Part 22: Linear Profile Filters: Spline Filters. Polish Committee for Standardization: Warsaw, Poland, 2015.
20. *PN-EN ISO 16610-28*; Geometrical Product Specifications (GPS), Filtration, Part 28: Profile Filters: End Effects. Polish Committee for Standardization: Warsaw, Poland, 2017.
21. *PN-EN ISO 16610-29*; Geometrical Product Specifications (GPS), Filtration, Part 29: Linear Profile Filters: Wavelets. Polish Committee for Standardization: Warsaw, Poland, 2020.
22. *PN-EN ISO 16610-31*; Geometrical Product Specifications (GPS), Filtration, Part 31: Robust Profile Filters: Gaussian Regression Filters. Polish Committee for Standardization: Warsaw, Poland, 2017.
23. *PN-EN ISO 16610-41*; Geometrical Product Specifications (GPS), Filtration, Part 41: Morphological Profile Filters: Disk and Horizontal Line-Segment Filters. Polish Committee for Standardization: Warsaw, Poland, 2015.
24. *PN-EN ISO 16610-49*; Geometrical Product Specifications (GPS), Filtration, Part 49: Morphological Profile Filters: Scale Space Techniques. Polish Committee for Standardization: Warsaw, Poland, 2015.
25. *PN-EN ISO 16610-61*; Geometrical Product Specifications (GPS), Filtration, Part 61: Linear Areal Filters: Gaussian Filters. Polish Committee for Standardization: Warsaw, Poland, 2015.
26. *PN-EN ISO 16610-62*; Geometrical Product Specifications (GPS), Filtration, Part 62: Linear Areal Filters: Spline Filters. Polish Committee for Standardization: Warsaw, Poland, 2023.
27. *PN-EN ISO 16610-71*; Geometrical Product Specifications (GPS), Filtration, Part 71: Robust Areal Filters: Gaussian Regression Filters. Polish Committee for Standardization: Warsaw, Poland, 2015.
28. *PN-EN ISO 16610-85*; Geometrical Product Specifications (GPS), Filtration, Part 85: Morphological Areal Filters: Segmentation. Polish Committee for Standardization: Warsaw, Poland, 2013.
29. Whitehouse, D.J. *Handbook of Surface Metrology*, 1st ed.; CRC Press: New York, NY, USA, 1994.
30. Dobrzanski, P.; Pawlus, P. Digital filtering of surface topography: Part I. Separation of one-process surface roughness and waviness by Gaussian convolution, Gaussian regression and spline filters. *Precis. Eng.* **2010**, *34*, 647–650. [CrossRef]
31. Kondo, Y.; Yoshida, I.; Nakaya, D.; Numada, M.; Koshimizu, H. Verification of characteristics of Gaussian filter series for surface roughness in ISO and proposal of filter selection guidelines. *Nanomanuf. Metrol.* **2021**, *4*, 97–108. [CrossRef]
32. *PN-EN ISO 3274*; Geometrical Product Specifications (GPS), Surface Texture: Profile Method, Nominal Characteristics of Contact (Stylus) Instruments. Polish Committee for Standardization: Warsaw, Poland, 2011.

33. Wang, Z.; Meng, H.; Fu, J. Novel method for evaluating surface roughness by grey dynamic filtering. *Measurement* **2010**, *43*, 78–82. [CrossRef]
34. Le Goïc, G.; Bigerelle, M.; Samper, S.; Favrelière, H.; Pillet, M. Multiscale roughness analysis of engineering surfaces: A comparison of methods for the investigation of functional correlations. *Mech. Syst. Signal Process.* **2016**, *66–67*, 437–457. [CrossRef]
35. Eseholi, T.; Coudoux, F.-X.; Corlay, P.; Sadli, R.; Bigerelle, M. A multiscale topographical analysis based on morphological information: The HEVC multiscale decomposition. *Materials* **2020**, *13*, 5582. [CrossRef]
36. He, B.; Zheng, H.; Ding, S.; Yang, R.; Shi, Z. A review of digital filtering in evaluation of surface roughness. *Metrol. Meas. Syst.* **2021**, *28*, 217–253. [CrossRef]
37. Pérez-Ruiz, J.D.; de Lacalle, L.N.L.; Urbikain, G.; Pereira, O.; Martínez, S.; Bris, J. On the relationship between cutting forces and anisotropy features in the milling of LPBF Inconel 718 for near net shape parts. *Int. J. Mach. Tools Manuf.* **2021**, *170*, 103801. [CrossRef]
38. Pérez-Ruiz, J.D.; Marin, F.; Martínez, S.; Lamikiz, A.; Urbikain, G.; de Lacalle, L.N.L. Stiffening near-net-shape functional parts of Inconel 718 LPBF considering material anisotropy and subsequent machining issues. *Mech. Syst. Signal Process.* **2022**, *168*, 108675. [CrossRef]
39. Matuszak, M.; Garbellini, A.; Powałka, B.; Attanasio, A.; Bachtiak-Radka, E. Accuracy analysis of the micro-milling process. *J. Mach. Constr. Maint.* **2017**, *107*, 37–43.
40. Pour, M. Determining surface roughness of machining process types using a hybrid algorithm based on time series analysis and wavelet transform. *Int. J. Adv. Manuf. Technol.* **2018**, *97*, 2603–2619. [CrossRef]
41. Lucas, K.; Sanz-Lobera, A.; Antón-Acedos, P.; Amatriain, A. A survey of bidimensional wavelet filtering in surface texture characterization. *Procedia Manuf.* **2019**, *41*, 811–818. [CrossRef]
42. Zmarzły, P. Influence of bearing raceway surface topography on the level of generated vibration as an example of operational heredity. *Indian J. Eng. Mater. Sci.* **2020**, *27*, 356–364.
43. Prabhakar, D.V.N.; Kumar, M.S.; Krishna, A.G. A Novel Hybrid Transform approach with integration of Fast Fourier, Discrete Wavelet and Discrete Shearlet Transforms for prediction of surface roughness on machined surfaces. *Measurement* **2020**, *164*, 108011. [CrossRef]
44. Gogolewski, D. Fractional spline wavelets within the surface texture analysis. *Measurement* **2021**, *179*, 109435. [CrossRef]
45. Dutta, S.; Pal, S.K.; Sen, R. Progressive tool flank wear monitoring by applying discrete wavelet transform on turned surface images. *Measurement* **2016**, *77*, 388–401. [CrossRef]
46. Wang, X.; Shi, T.; Liao, G.; Zhang, Y.; Hong, Y.; Chen, K. Using wavelet packet transform for surface roughness evaluation and texture extraction. *Sensors* **2017**, *17*, 933. [CrossRef]
47. Sun, J.; Song, Z.; He, G.; Sang, Y. An improved signal determination method on machined surface topography. *Precis. Eng.* **2018**, *51*, 338–347. [CrossRef]
48. Josso, B.; Burton, D.R.; Lalor, M.J. Frequency normalised wavelet transform for surface roughness analysis and characterisation. *Wear* **2002**, *252*, 491–500. [CrossRef]
49. Zahouani, H.; Mezghani, S.; Vargiolu, R.; Dursapt, M. Identification of manufacturing signature by 2D wavelet decomposition. *Wear* **2008**, *264*, 480–485. [CrossRef]
50. Gogolewski, D.; Makieła, W.; Stępień, K.; Zmarzły, P.; Wrzochal, M. The Assessment of Wavelet Transform Parameters Regarding its Use in 3D Surface Filtering. In Proceedings of the 29th DAAAM International Symposium on Intelligent Manufacturing and Automation, Zadar, Croatia, 24–27 October 2018; pp. 1191–1196.
51. Shao, Y.; Du, S.; Tang, H. An extended bi-dimensional empirical wavelet transform based filtering approach for engineering surface separation using high definition metrology. *Measurement* **2021**, *178*, 109259. [CrossRef]
52. Daffara, C.; Mazzocato, S.; Marchioro, G. Multiscale roughness analysis by microprofilometry based on conoscopic holography: A new tool for treatment monitoring in highly reflective metal artworks. *Eur. Phys. J. Plus* **2022**, *137*, 430. [CrossRef]
53. Beck, T.W.; DeFreitas, J.M.; Cramer, J.T.; Stout, J.R. A comparison of adaptive and notch filtering for removing electromagnetic noise from monopolar surface electromyographic signals. *Physiol. Meas.* **2009**, *30*, 353. [CrossRef]
54. Lu, G.; Brittain, J.-S.; Holland, P.; Yianni, J.; Green, A.L.; Stein, J.F.; Aziz, T.Z.; Wang, S. Removing ECG noise from surface EMG signals using adaptive filtering. *Neurosci. Lett.* **2009**, *462*, 14–19. [CrossRef]
55. Lou, S.; Tang, D.; Zeng, W.; Zhang, T.; Gao, F.; Muhamedsalih, H.; Jiang, X.; Scott, P.J. Application of clustering filter for noise and outlier suppression in optical measurement of structured surfaces. *IEEE Trans. Instrum. Meas.* **2020**, *69*, 6509–6517. [CrossRef]
56. Podulka, P. Reduction of influence of the high-frequency noise on the results of surface topography measurements. *Materials* **2021**, *14*, 333. [CrossRef]
57. Li, Z.; Gröger, S. Investigation of noise in surface topography measurement using structured illumination microscopy. *Metrol. Meas. Syst.* **2021**, *28*, 767–779. [CrossRef]
58. *PN-EN ISO 25178-2*; Geometrical Product Specifications (GPS), Surface Texture: Areal, Part 2: Terms, Definitions and Surface Texture Parameters. Polish Committee for Standardization: Warsaw, Poland, 2022.
59. Grochała, D.; Berczyński, S.; Grządziel, Z. Analysis of surface geometry changes after hybrid milling and burnishing by ceramic ball. *Materials* **2019**, *12*, 1179. [CrossRef] [PubMed]
60. Rodriguez, A.; de Lacalle, L.N.L.; Pereira, O.; Fernandez, A.; Ayesta, I. Isotropic finishing of austempered iron casting cylindrical parts by roller burnishing. *Int. J. Adv. Manuf. Technol.* **2020**, *110*, 753–761. [CrossRef] [PubMed]

61. Pappas, A.; Newton, L.; Thomson, A.; Hooshmand, H.; Leach, R. Uncertainty Propagation of Field Areal Surface Texture Parameters Using the Metrological Characteristics Approach. In Proceedings of the EuSPEN's 23rd International Conference & Exhibition, Copenhagen, Denmark, 12–16 June 2023.
62. Selesnick, I.W.; Baraniuk, R.G.; Kingsbury, N.C. The dual-tree complex wavelet transform. *IEEE Signal Process. Mag.* **2005**, *22*, 123–151. [CrossRef]
63. Jiang, X.; Scott, P.; Whitehouse, D. Wavelets and their applications for surface metrology. *CIRP Ann.* **2008**, *57*, 555–558. [CrossRef]
64. Whitehouse, D.J. *Handbook of Surface and Nanometrology*, 2nd ed.; CRC Press: Boca Raton, FL, USA, 2011.
65. García Plaza, E.; Núñez López, P.J. Application of the wavelet packet transform to vibration signals for surface roughness monitoring in CNC turning operations. *Mech. Syst. Signal Process.* **2018**, *98*, 902–919. [CrossRef]
66. Donoho, D.L.; Johnstone, I.M.; Kerkyacharian, G.; Picard, D. Wavelet shrinkage: Asymptopia? *J. R. Stat. Soc. Ser. B Stat. Methodol.* **1995**, *57*, 301–337. [CrossRef]
67. Murtagh, F.; Starck, J.-L. Image processing through multiscale analysis and measurement noise modeling. *Stat. Comput.* **2000**, *10*, 95–103. [CrossRef]
68. Fu, S.; Muralikrishnan, B.; Raja, J. Engineering surface analysis with different wavelet bases. *J. Manuf. Sci. Eng.* **2003**, *125*, 844–852. [CrossRef]